Bifunctional Materials

DOI: 10.1002/anie.201209884

Magnetic Tuning of Upconversion Luminescence in Lanthanide-Doped Bifunctional Nanocrystals**

Yunxin Liu, Dingsheng Wang, Jianxin Shi, Qing Peng, and Yadong Li**

Optical-magnetic (OM) bifunctional materials are of great interest for developing advanced multifunctional devices.[1–4] Conventional OM bifunctional materials are composites that are produced by coupling optical materials with magnetic ones. It is very difficult to realize an interaction between the optical and magnetic properties (e.g., tuning the optical properties using a magnetic field) in these conventional OM materials because of the separation of the optical and magnetic phases. On the other hand, producing materials with OM interactions would be valuable for developing advanced OM devices for high-accuracy communications, aircraft guidance, and magnetic field detection.[4–7] OM interactions depend mainly on the outermost electrons and thus, occur at the atomic scale. To achieve an OM interaction, a single-phase material should simultaneously have optical and magnetic properties to ensure the OM interaction occurs between atoms in the same crystal lattice, not at the interface between two separated phases with a high density of defects.

Recent reports show that OM interactions can be simultaneously observed in single-crystal or single-phase materials by lanthanide (Ln) doping, for example, $NaGdF_4$:Yb^{3+},Er^{3+}[8,9] and Gd_2O_3:Yb^{3+},Er^{3+}.[6,10] The host materials containing Gd^{3+} ions have paramagnetic properties while the doped Er^{3+} ions form luminescent centers.[6,8–10] The luminescence of Er^{3+} ions depends on their coordinated magnetic ion, Gd^{3+}. Therefore, if the impact of the coordinating magnetic ions on their luminescent centers is strong enough, they should change the luminescence of these lanthanide-doped materials depending on the magnetic field.

In comparison to Gd_2O_3, $NaGdF_4$ has a lower matrix phonon energy so that it generates a higher luminescent efficiency.[11] Moreover, for $NaLnF_4$ structures, heavy doping of other lanthanide ions does not usually generate precipitating phases. Considering its advantages, we chose $NaGdF_4$ as the host material to dope with the classic upconversion ionic pair, Yb^{3+}/Er^{3+}, which can convert low-energy infrared (IR) photons to higher-energy visible light. To adjust the OM properties, an Nd^{3+} ion was introduced into the $NaGdF_4$:Yb^{3+},Er^{3+} system. As shown in Figure 1a, the crystal structure of hexagonal $NaGdF_4$ consists of one ninefold coordinated site occupied randomly by Na^+ and Gd^{3+} ions with a site symmetry of C_{3h}. After doping with Nd^{3+}, Yb^{3+}, and Er^{3+} ions, a portion of the Gd^{3+} ions will be substituted in the C_{3h} sites (see Figure 1b). Notably, the doping of Yb^{3+}/Er^{3+} ion pairs will lead to shrinkage of the $NaGdF_4$ crystal lattices because the doped Yb^{3+}/Er^{3+} (r = 1.125/1.144 Å)[12] ion pairs have a smaller ionic radius than the host Gd^{3+} (r = 1.193 Å)[12] ion. In contrast, doping with Nd^{3+} ions leads to the stretching of the $NaGdF_4$ crystal lattices because of the relatively larger ionic radius of the Nd^{3+} (r = 1.249 Å) ion.[12] Thus, doping with Nd^{3+}, Yb^{3+}, and Er^{3+} ions considerably changes the symmetry of the C_{3h} sites in the $NaGdF_4$ crystal lattices. On the other hand, the luminescent properties of the Er^{3+} ion and the magnetic properties of the $NaGdF_4$ host are both dependent on the symmetry of the C_{3h} sites. So the OM properties of $NaGdF_4$ can be simultaneously tuned by controlling the amount of doping.

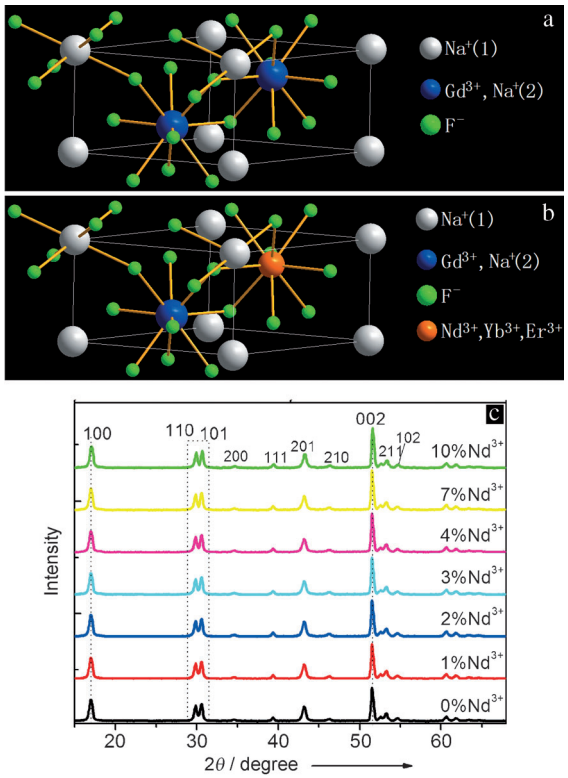

Figure 1. Scheme of the hexagonal-phase $NaGdF_4$ structures a) undoped and b) doped with Nd^{3+},Yb^{3+},Er^{3+} ions. c) XRD spectra of $NaGdF_4$:x%Nd^{3+},20%Yb^{3+},2%Er^{3+} (x = 0, 1, 2, 3, 4, 7, 10).

[*] Dr. Y. Liu, Dr. D. Wang, J. Shi, Dr. Q. Peng, Prof. Y. Li
Department of Chemistry, Tsinghua University
Beijing 100084 (China)
E-mail: pengqing@tsinghua.edu.cn
ydli@tsinghua.edu.cn

[**] This work was supported by the State Key Project of Fundamental Research for Nanoscience and Nanotechnology (2011CB932401 and 2011CBA00500) and the National Natural Science Foundation of China (Grant No. 20921001 and 21131004).

Supporting information for this article is available on the WWW under http://dx.doi.org/10.1002/anie.201209884.

High quality $NaGdF_4$:Nd^{3+},Yb^{3+},Er^{3+} nanocrystals were synthesized using a solvothermal method in an oleic acid (OA)/octadecene (ODE) system.[13–16] X-ray diffraction patterns (Figure 1c) indicate that the synthesized samples have hexagonal crystal structures with the preferred crystallographic orientation along the *c* axis. By increasing the concentration of Nd^{3+} ions from 0 to 10 mol%, no precipitating phase or cubic transition phase was observed, demonstrating the successful substitution of Gd^{3+} ions by Nd^{3+}, Yb^{3+}, and Er^{3+} ions in the C_{3h} sites.

TEM images in Figure 2 show that $NaGdF_4$:3%Nd^{3+},20%Yb^{3+},2%Er^{3+} has a nanoplate morphology, uniform particle size, and a diameter to thickness ratio of two. The HRTEM image (Figure 2c) shows the single-crystal nature of these nanoplates. Combining the XRD and HRTEM results, the surfaces of these nanoplates are shown to be perpendicular to the *c* axis (the preferred crystallographic orientation; Figure 2b).[16] Because of their high monodispersity, these uniform $NaGdF_4$ nanoplates can be easily deposited into ultra-smooth films with various ordered structures, such as bifunctional film perpendicular to *c* axis (BFEC, Figure 2d,g), bifunctional film parallel to *c* axis (BFAC, Figure 2e,h), and bifunctional superlattice (BFSL, Figure 2f,i) structures.

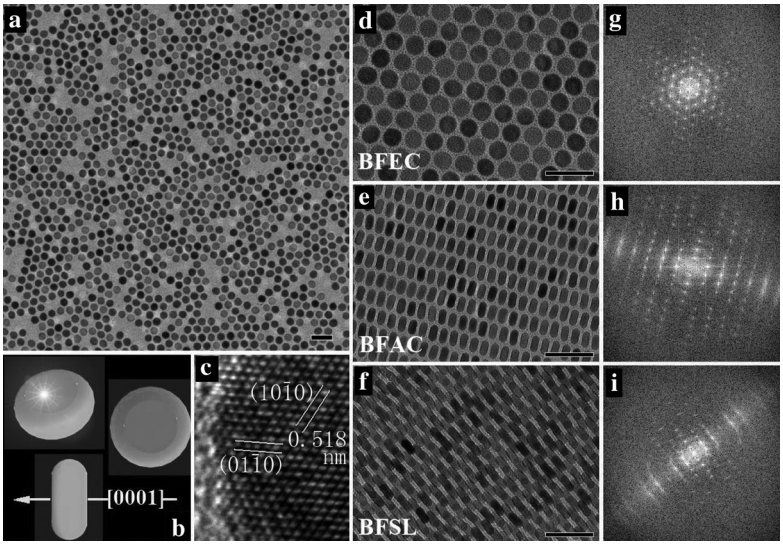

Figure 2. a) TEM image, b) shape models, and c) HRTEM image of $NaGdF_4$:3%Nd^{3+},20%Yb^{3+},2%Er^{3+} nanoplates. TEM image (d–f) and corresponding fast fourier-transform (g–i) of d,g) BFEC, e,h) BFAC, and f,i) BFSL. All scale bars = 50 nm.

To demonstrate the OM interaction, $NaGdF_4$:3%Nd^{3+}, 20%Yb^{3+}, 2%Er^{3+} BFSL with both upconversion luminescence and paramagnetism (Supporting Information, Figures S1–S3) was used to investigate the tuning of upconversion luminescence by a magnetic field. BFSL on a substrate was placed in a magnetic field perpendicular to the surface of the BFSL film (Figure 3a). The IR excitation light with a wavelength of 980 nm was delivered to the BFSL surface using an optical fiber, while the visible emissions were collected by another optical fiber. Figure 3c shows that the green emission from the $4f^n$ shell electronic transition $^4S_{3/2}/^2H_{11/2}\rightarrow{}^4I_{15/2}$ of the Er^{3+} ion can be efficiently tuned by changing the applied magnetic field at room temperature (300 K). When the applied magnetic field reached up to 12 KO_e, the integral luminescent intensity could decrease to ≈60% of the original value. This magnetic tuning effect of the upconvertion luminescence was found to be more remarkable as BFSL cooled down to 10 K (Figure 3d). When the applied magnetic field reached 12 kOe ($1\ Oe = 12.56\ kA\,m^{-1}$), the integral luminescent intensity decreased to approximately 15% of the original value, at the ultralow temperature of 10 K. After removal of the applied magnetic field, the integral intensity of upconversion luminescence recovered, with loss lower than 5% for more than 50 cycles (Figure S4).

When the amount of Nd^{3+} doping was varied, we observed that the corresponding magnetic tuning efficiency of upconversion luminescence of the BFSL could be adjusted, especially at low temperature (Figure 3e,f). At 10 K, the magnetic tuning efficiency of upconversion luminescence increased by 50% with 4 mol% Nd^{3+} ion doping (Figure 3f and Supporting Information, Part III). Notably, the influence of Nd^{3+} doping on the magnetic tuning efficiency is nonlinear. For a fixed composition of 20 mol% Yb^{3+} and 2 mol% Er^{3+} ions, the optimal doping concentration of Nd^{3+} was approximately 4 mol%, while further increases of Nd^{3+} doping lead to a decrease in magnetic tuning efficiency.

To address whether this OM interaction can be observed in a material with only optical properties, $NaYF_4$:*x*Nd^{3+},20%Yb^{3+},2%Er^{3+} (x = 0–4 mol%, no detectable paramagnetic properties at room temperature) was synthesized with the same procedure as $NaGdF_4$. Under an applied magnetic field up to 12 kOe, the upconversion luminescence of $NaYF_4$:*x* Nd^{3+},20%Yb^{3+},2%Er^{3+} (x = 0–4 mol%) showed no change at room temperature (Figure 3g). At 10 K (Figure 3h), the upconversion luminescence of $NaYF_4$:4%Nd^{3+},20%Yb^{3+},2%Er^{3+} showed a slight decrease in integral intensity. The magnetization curves indicated that $NaYF_4$:4%Nd^{3+},20%Yb^{3+},2%Er^{3+} has detectable paramagnetic properties at 10 K (Figure S5). From this, we concluded that a single-phase material possessing both optical and magnetic properties is necessary for detectable OM interactions at a given temperature and magnetic field.

Magnetic tuning of the green emission is mainly due to the splitting of $^4S_{3/2}$ level into four Zeeman levels, $|-3/2\rangle$, $|+3/2\rangle$, $|-1/2\rangle$, and $|+1/2\rangle$ (Figure 4a). The gap between the lowest levels $|-3/2\rangle$ and $|-1/2\rangle$ increases with increasing applied magnetic field, which leads to a larger splitting of the $|\pm 3/2\rangle$ doublet, then to a negligible radiative probability from $|-3/2\rangle$ and $|+3/2\rangle$. On the other hand, most of the emission comes from the lowest $|-3/2\rangle$ level in the $^4S_{3/2}$ quartet. Therefore, an applied magnetic field decreases the total luminescent intensity from the $^4S_{3/2}$ quartet.[5] To verify the influence of Nd^{3+} doping on the optical properties of $NaGdF_4$:Yb,Er, the dependence of the green emission on excitation power was

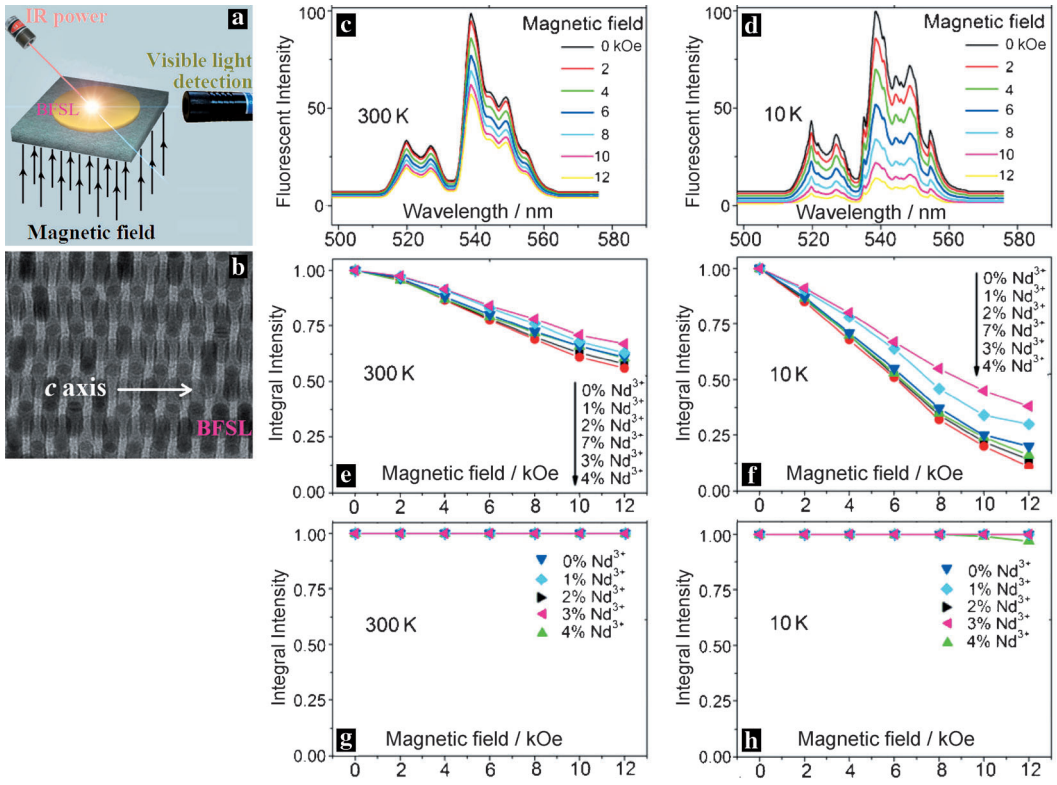

Figure 3. a) Scheme of the magnetic tuning process of upconversion luminescence in $NaGdF_4$:Nd,Yb,Er BFSL. b) BFSL film parallel to the *c* axis. Effect of external magnetic field on the green emission of Er^{3+} ions in $NaGdF_4$:Nd,Yb,Er BFSL at c) 300 K and d) 10 K. Dependence of the integral emission intensity of $NaGdF_4$:Nd,Yb,Er BFSL with various levels of Nd^{3+} doping on the applied magnetic field at e) 300 K and f) 10 K. Dependence of the integral emission intensity of $NaYF_4$:Nd,Yb,Er with various levels of Nd^{3+} doping on the applied magnetic field at g) 300 K and h) 10 K.

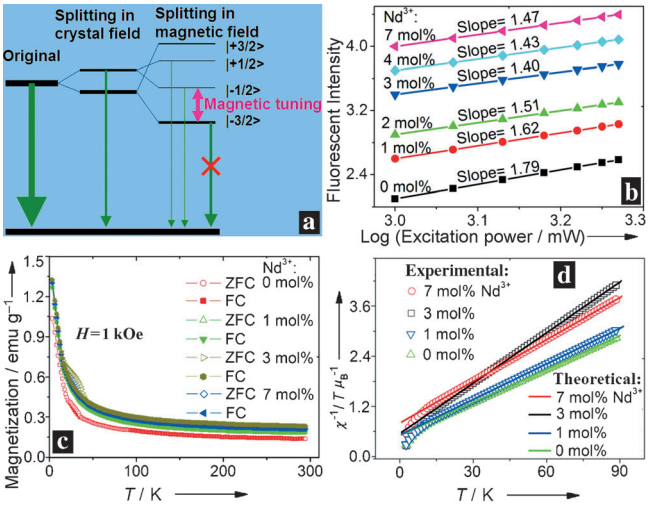

Figure 4. a) The splitting of energy level $^4S_{3/2}$ of the Er^{3+} ion in which the gap between the Zeeman levels $|-1/2\rangle$ and $|-3/2\rangle$ increases with applied magnetic field. b) Plot of the dependence of upconversion luminescence intensity of $NaGdF_4$:x%Nd^{3+},20%Yb^{3+},2%Er^{3+} (x=0, 1, 2, 3, 4, 7) on the excitation power. c) Zero-field-cooled (ZFC) and field-cooled (FC) magnetization of $NaGdF_4$:x%Nd^{3+},20%Yb^{3+},2%Er^{3+} (x=0, 1, 3, 7). d) Experimental and theoretical temperature dependence of the inverse magnetic susceptibility of $NaGdF_4$:x%Nd^{3+},20%Yb^{3+},2%Er^{3+} (x=0, 1, 3, 7).

measured, treated by Auzel's method, $I \approx P^n$ (I = intensity, P = excitation power, and n = fitting slope),[17] and presented in Figure 4b. The n-value for green emission decreased from 1.79 to 1.47 with increasing Nd^{3+} ions (0–7 mol%), demonstrating the saturation effect of the $^4I_{11/2}$ state of the Er^{3+} ion induced by Nd^{3+} doping. Based on a simplified energy-level diagram (Figure S6), we suggest that the cross relaxation between Er^{3+} and Nd^{3+} ions of $^4I_{13/2}(Er) + {}^4I_{13/2}(Nd) \rightarrow {}^4I_{11/2}(Er) + {}^4I_{15/2}(Nd)$ contributes to the remarkable enhancement of the $^4I_{11/2}$ state population of Er^{3+} ions.[18]

Nd^{3+} doping also had a remarkable influence on the magnetic properties of the $NaGdF_4$ host. Both room and ultralow temperature magnetization of $NaGdF_4$ was enhanced by doping with Nd^{3+} ions (Figure 4c). This tuning of magnetic properties was shown to be nonlinear. At a low doping level (0–3 mol%) of Nd^{3+} ions, the coordinating field symmetry of Gd^{3+} ions was lower because of a deviation of the atomic radius (0.056 Å) and a different outermost electron distribution ($Nd:4f^46s^2$, $Gd:4f^75d^16s^2$). Alternatively, at higher doping levels (7–10 mol%), ordered $NaGdF_4$ crystal lattices can break down[19] so that some localized states of Gd^{3+} ions are formed, resulting in lower magnetic susceptibility. This was shown by the dependence of magnetic susceptibility on the level of Nd^{3+} doping (Figure 4d).

Usually, the magnetic susceptibility, $X(T)$, of bulk paramagnetic materials obeys the Curie or Curie–Weiss law with temperature (T) variation: $X(T) = C/(T-\theta)$, where C = Curie constant and θ = Curie–Weiss temperature.[20] We fitted the experimental susceptibilities with the Curie–Weiss equation (Figure 4d). Surprisingly, the inverse susceptibility of $NaGdF_4$:x%Nd^{3+},20%Yb^{3+},2%Er^{3+} (x=0, 1, 3, 7 mol%) at low temperature (T < 20 K) deviates from the Curie–Weiss fit curve. Figure 4c shows maxima in the zero-field-cooled (ZFC) magnetization curves for $NaGdF_4$: x%Nd^{3+},20%Yb^{3+},2%Er^{3+} (x=0, 1, 3, 7 mol%) at 25.2, 25.0, 24.6, and 24.3 K, respectively (enlarged in Figure S7),

which are often referred to as the blocking temperature (T_B).[20] Materials with smaller particle sizes have a lower T_B value.[20] The T_B value of bulk materials should be much higher than thin nanocrystals (less than 25 nm) so that an ultralow T_B occurs only for thin nanocrystals. Below the T_B, the inverse magnetic susceptibility takes an exponential variation instead of following the Curie–Weiss law.[20] This is the main reason for the deviation from the Curie–Weiss curve of $NaGdF_4$:Nd^{3+},Yb^{3+},Er^{3+} at low temperature ($T < 20$ K). Furthermore, the magnetic tuning efficiency of BFEC (Figure 2d) at 10 K was slightly lower than that for BFAC (Figure 2e) and BFSL (Figure 2f; see Figure S8), but the mechanism involved in this observation needs further investigation.

In conclusion, OM bifunctional $NaGdF_4$:Nd^{3+},Yb^{3+},Er^{3+} nanocrystals were successfully synthesized, consisting of a luminescent center Er^{3+} ion and a coordinating magnetic ion, Gd^{3+}. Upconversion luminescence of $NaGdF_4$:Nd^{3+},Yb^{3+},Er^{3+} was efficiently tuned by applying a magnetic field both at room and ultralow temperature; this was due to an increase in the energy gaps between splitting sub-levels with increasing applied magnetic field. The magnetic tuning efficiency of upconversion luminescence can be adjusted by varying the amount of Nd^{3+} doping. For a 3 mol% Nd^{3+} doped sample, the integral intensity of upconversion luminescence under an applied magnetic field of 12 kOe decreased to approximately 15% of the original value at 10 K. After removal of the applied magnetic field, the integral intensity of upconversion luminescence recovered with less than 5% loss over more than 50 cycles. This bifunctional material with controllable OM interactions has potential applications in high accuracy communications, aircraft guidance, and optical- and magnetic-field detection.

Experimental Section

Synthesis of 20 nm $NaGdF_4$:3%Nd^{3+},20%Yb^{3+},2%Er^{3+} nanoplates: $Gd(CF_3COOH)_3$ (0.75 mmol), $Nd(CF_3COOH)_3$ (0.03 mmol), $Yb(CF_3COOH)_3$ (0.2 mmol), $Er(CF_3COOH)_3$ (0.02 mmol), and $Na(CF_3COOH)$ (6 mmol) were combined with ODE (10 mL) and OA (10 mL) in a three-necked flask. The mixture was heated under vacuum at 110°C for 40 min to give a transparent solution. Subsequently, the reaction flask was flushed with N_2 for 10 min to remove residual water and oxygen and then heated to 330°C for 50 min under argon gas. Following the reaction, the solution was cooled by adding ODE (10 mL). Products were isolated by adding ethanol and centrifuging the mixture. The products could be redispersed in a nonpolar solvent. The morphology and size of the products could be tuned by varying the reaction temperature and time and the concentration of Ln^{3+} ions (see Supporting Information).

BFEC was formed by quickly depositing the nanocrystal hexane solution onto the substrate. BFAC was formed by quickly depositing the nanocrystal chloroform solution onto the substrate. BFSL was formed by depositing the nanocrystal hexane solution onto the substrates with N_2 flowing between the surfaces of the substrates.

Measurement of the magnetic tuning of upconversion luminescence: BFSL on a non-magnetic substrate was placed in a cryostat, wherein the temperature could be varied from 300 K to 10 K. A liquid-helium-cooled superconductor coil was used with a DC magnetic field, perpendicular to the surface of the BFSL film. The IR excitation light (wavelength = 980 nm) was delivered to the BFSL using an optical fiber, and the visible light emission was collected by another optical fiber. The upconversion luminescent spectra were acquired using a fiber-optically coupled F4500 fluorescence spectrometer.

The morphology of the synthesized samples was measured using a Hitachi HT-7700 transmission electron microscope. High-resolution TEM (HRTEM) was performed using an FEI Tecnai G2 F20 S-Twin electron microscope. Powder X-ray diffraction patterns were recorded using a Bruker D8 Advance X-ray powder diffractometer with Cu Kα radiation ($\lambda = 1.5406$ Å). Magnetic studies were carried out on a MPMS Quantum Design superconducting quantum interference device (SQUID) magnetometer.

Received: December 11, 2012
Revised: February 1, 2013
Published online: March 19, 2013

Keywords: lanthanides · luminescence · magnetic properties · nanocrystals · optical-magnetic materials

[1] J. L. Bridot, A. C. Faure, S. Laurent, C. Rivière, C. Billotey, B. Hiba, M. Janier, V. Josserand, J. L. Coll, L. Vander Elst, R. Muller, S. Roux, P. Perriat, O. Tillement, *J. Am. Chem. Soc.* **2007**, *129*, 5076.
[2] H. Kim, M. Achermann, L. P. Balet, J. A. Hollingsworth, V. I. Klimov, *J. Am. Chem. Soc.* **2005**, *127*, 544.
[3] H. Gu, R. Zheng, X. Zhang, B. Xu, *J. Am. Chem. Soc.* **2004**, *126*, 5664.
[4] G. F. Wang, Q. Peng, Y. D. Li, *Acc. Chem. Res.* **2011**, *44*, 322.
[5] V. K. Tikhomirov, L. F. Chibotaru, D. Saurel, P. Gredin, M. Mortier, V. V. Moshchalkov, *Nano Lett.* **2009**, *9*, 721.
[6] S. K. Singh, K. Kumar, M. K. Srivastava, D. K. Rai, S. B. Rai, *Opt. Lett.* **2010**, *35*, 1575.
[7] R. Valiente, M. Millot, F. Rodríguez, J. González, J. M. Broto, S. George, S. García-Revilla, Y. Romanyuk, M. Pollnau, *High Pressure Res.* **2009**, *29*, 748.
[8] Z. L. Wang, J. H. Hao, H. L. W. Chan, *J. Mater. Chem.* **2010**, *20*, 3178.
[9] D. Wang, L. Ren, X. Zhou, X. Wang, J. Zhou, Y. Han, N. Kang, *Nanotechnology* **2012**, *23*, 225705.
[10] C. B. Tan, B. Ma, J. Zhang, Y. Zuo, W. Zhu, Y. X. Liu, W. B. Li, Y. T. Zhang, *Mater. Lett.* **2012**, *73*, 147.
[11] F. Wang, X. G. Liu, *Chem. Soc. Rev.* **2009**, *38*, 976.
[12] R. D. Shannon, *Acta Crystallogr. Sect. A* **1976**, *32*, 751.
[13] J. C. Boyer, F. Vetrone, L. A. Cuccia, J. A. Capobianco, *J. Am. Chem. Soc.* **2006**, *128*, 7444.
[14] R. Abdul Jalil, Y. Zhang, *Biomaterials* **2008**, *29*, 4122.
[15] F. Wang, J. Wang, X. G. Liu, *Angew. Chem.* **2010**, *122*, 7618; *Angew. Chem. Int. Ed.* **2010**, *49*, 7456.
[16] X. C. Ye, J. E. Collins, Y. J. Kang, J. Chen, D. T. N. Chen, A. G. Yodh, C. B. Murray, *Proc. Natl. Acad. Sci. USA* **2010**, *107*, 22430.
[17] F. Auzel, *Proc. IEEE* **1973**, *61*, 758.
[18] F. Wang, Y. Han, C. S. Lim, Y. H. Lu, J. Wang, J. Xu, H. Y. Chen, C. Zhang, M. H. Hong, X. G. Liu, *Nature* **2010**, *463*, 1061.
[19] D. T. Tu, Y. S. Liu, H. M. Zhu, R. F. Li, L. Q. Liu, X. Y. Chen, *Angew. Chem.* **2013**, *125*, 1166; *Angew. Chem. Int. Ed.* **2013**, *52*, 1128.
[20] W. Van den Heuvel, V. K. Tikhomirov, D. Kirilenko, N. Schildermans, L. F. Chibotaru, J. Vanacken, P. Gredin, M. Mortier, G. van Tendeloo, V. V. Moshchalkov, *Phys. Rev. B* **2010**, *82*, 094421.

